VULNERABILITY OF SHIELDED FUEL PIPES AND HEAT PIPES TO HYPERVELOCITY IMPACTS

Robin Putzar[(1)], Frank Schäfer[(1)], Oliver Romberg[(2)], Michel Lambert[(3)]

[(1)] Fraunhofer Institute for High-Speed Dynamics (Ernst-Mach-Institut), Eckerstr. 4, D-79104 Freiburg, Germany, Email: putzar@emi.fhg.de, schaefer@emi.fhg
[(2)] OHB-System AG, Universitaetsallee 27-29, D-28359 Bremen, Germany, Email: romberg@ohb-system.de
[(3)] European Space Agency ESTEC, Keplerlaan 1, 2201 AZ Noordwijk, The Netherlands, Email: Michel.Lambert@esa.int

ABSTRACT

The vulnerability of space qualified fuel pipes and heat pipes to hypervelocity impacts has been assessed. The equipment has been placed behind representative spacecraft structure walls and operated at simulated conditions (i. e. carrying pressurized water or N_2 gas). Several failure modes have been investigated, of which perforation has emerged as the most critical. Ballistic limit curves for failure mode "perforation" are presented and compared against the test results. Impact induced overpressure has been investigated. Impacts on structure walls at velocities below 7 km/s can generate highly inhomogeneous fragment clouds. When the equipment located behind the structure wall is laterally confined, the existing approach for determining the failure probability (perforation / no perforation limit) strongly underpredicts its vulnerability. An approach to deal with failure probability in this case is presented.

1. INTRODUCTION

Space debris and meteoroids protection requirements are presently formulated in terms of the probability of no penetration. This approach is driven by the lack of data available for assessing the internal damage following perforation of the external wall and leads to unnecessarily heavy structures.

Impact tests to assess the vulnerability of different S/C (spacecraft) subsystems (piping, pressure vessels, electronics boxes, harness, batteries) to HVI (hypervelocity impact) are currently being performed. In this paper, results from these investigatory tests are presented, damage and failure modes of the structures are investigated, and their failure thresholds are determined, allowing a more comprehensive assessment of satellite vulnerability.

1.1. Representative Spacecraft Components

Fuel Pipes

In many S/C applications feed lines transporting propellant with a pressure in the order of magnitude of 3 MPa can be found. These pressure lines are MOD (meteoroid and orbital debris) critical components due to their large amount of stored potential energy. Any impact of MOD particles may damage the lines, resulting in:

- cratering without leakage of fluid;
- perforation leading to leakage of fluid and potential loss of propulsion function; or
- catastrophic burst of the pressurized component, resulting in secondary damages and / or contamination / sublimation of other parts of the S/C (e. g. scientific optical instruments) by potentially aggressive fuel components.

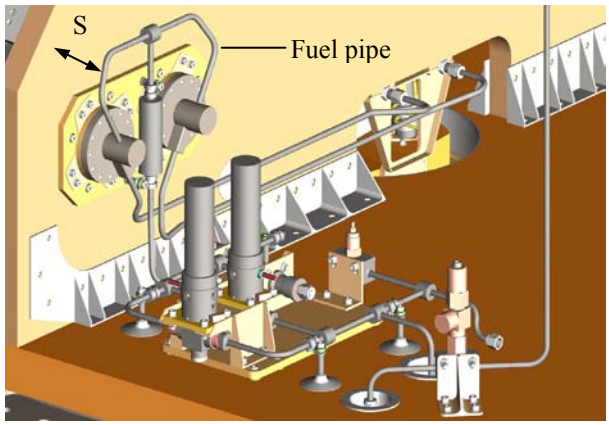

Figure 1. Typical configuration: FP routed inside a S/C with spacing S to the primary structure wall (a SP).

Depending on the individual S/C, FP (fuel pipes) can be routed barely outside the primary structure; protected behind a BP (bumper plate) (see e. g. Janovsky et al, 1999); or located inside the S/C with a varying spacing S to the primary structure (Fig. 1). FP commonly found in mid-sited S/C are of Ti3Al2.5V with a diameter of 6.4 mm, a wall thickness of 0.5 mm and contain hydrazine.

Heat Pipes

HP (heat pipes) (providing thermal control primarily for S/C electronic components) contain high-pressure (up to 4.5 MPa) NH_3 and N_2 depending on operational conditions. Penetration-inducing MOD particle impacts can result in:

- loss of working fluid and, therefore, loss of thermal control function (at least of the effected pipe);
- release of stored energy analogous to damaged FP.

In addition to accommodation analogous to FP, (e. g. Janovsky et al, 1999) various profile HP can be routed within a SP (sandwich panel) (see Fig. 2), routed through the S/C interior at variable distance to the BP or primary structure, or mounted directly to radiator panels (spacing S = 0).

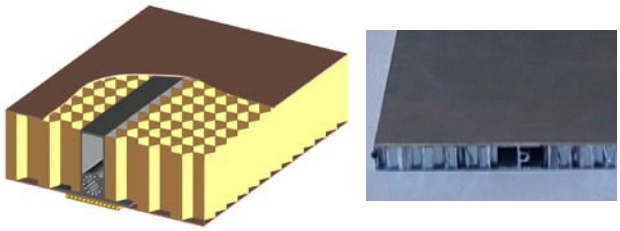

Figure 2. HP routed inside a H/C SP.

In the case of routing within a SP, the structural element serves as the primary structure, provides support for the HP, and acts as a radiator. HP are commonly of stainless steel with a diameter of ~10 mm.

2. TARGET DESCRIPTION

A majority of the equipment under investigation was tested behind representative S/C structure walls. The integrated HP and ACES HP were submitted to direct impacts (i. e. unshielded).

2.1. Structure Walls

Representative structural walls were selected for use in the impact test campaign (both BP and SP). The BP was an ATV-like plate: 0.81 mm (0.032") thick Al 6061 T6 (2700 kg/m^3); while the SP was MetOp-like: 0.41 mm (0.016") thick Al 2024 T3 (2760 kg/m^3) face sheets with a 35 mm thick 2.0-3/16-07P-5056-MIL-C-7438G H/C (honeycomb) core.

2.2. Fuel Pipes

The FP were manufactured according to SAE AMS 4945B with an outer diameter of 6.35 mm (0.25"), and a wall thickness of 0.41 mm (0.016"). They were of Ti-3Al-2.5V (4480 kg/m^3, minimum yield strength at 0.2% strain 724 MPa).

Three different configurations have been tested (Fig. 3): 25 mm stand-off from an ATV BP (referred to as "A25"); 50 mm and 100 mm stand-off from a MetOp H/C SP ("M50" and "M100" resp.). In front of both MetOp configurations MLI (Fig. 4) with an areal density of 0.447 kg/m^2 was mounted.

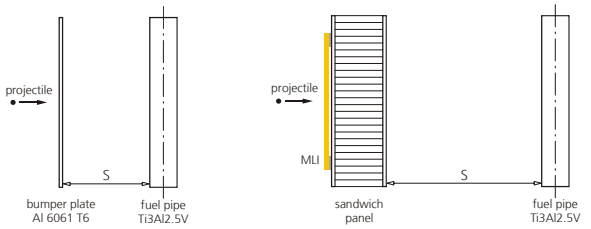

Figure 3. FP experimental set-ups. Left: A25, right: M50 and M100.

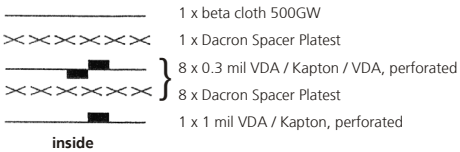

Figure 4. MLI lay-up.

2.3. Stand-alone Heat Pipes

The stand-alone HP are made of Al 6063 T5 (2710 kg/m^3, yield strength 130 MPa). The geometry is shown in Fig. 5. According to the manufacturer, the minimum wall thickness amounts to 0.82 – 0.95 mm.

Two different configurations have been tested (Fig. 6): 50 mm behind an ATV BP ("A50"); and 50 mm behind a MetOp H/C SP ("M50").

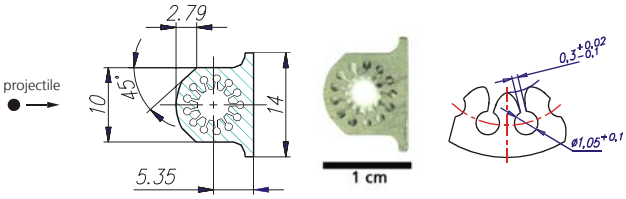

Figure 5. Stand-alone HP geometry.

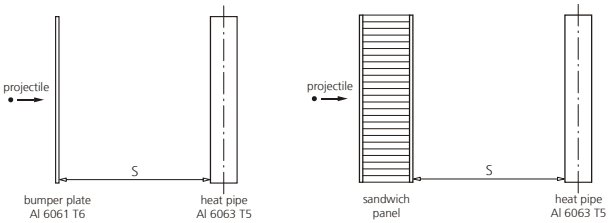

Figure 6. HP experimental set-ups. Left: A50, right: M50.

2.4. Integrated Heat Pipes

The integrated HP are made of Al 6063 T5 (see section 2.3). The geometry is shown in Fig. 7, groove geometry and minimum wall thickness is the same as in section 2.3. The integrated HP are embedded in an Al H/C SP with face sheets made of 1 mm thick Al 2024 (2780 kg/m^3, yield strength 270 MPa). The 20 mm thick SP H/C core specification is Hexcel 3/16-5056-0.0007. The mounting profile is made of Al 6063 T5 (same properties as HP), with a minimum thickness of 1.1 mm. The integrated HP have been impacted directly.

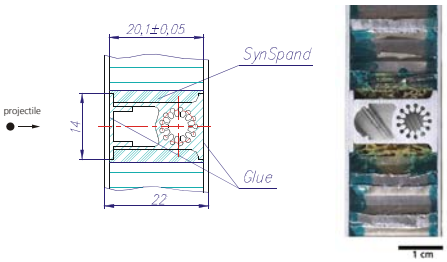

Figure 7. Integrated HP geometry.

2.5. ACES Heat Pipes

The ACES HP (Fig. 8) are made of Al 3.3206 (2700 kg/m^3, yield strength 160 MPa). Minimum wall thickness is 1.0 mm. They are embedded in an Al H/C SP with 0.3 mm thick Al 7075 T7351 face sheets (2710 kg/m^3, tensile yield stress 386.1 MPa). The H/C core specification is 3/16-5056-0.001P. The ACES HP have been impacted directly.

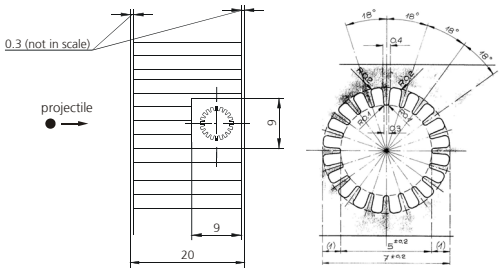

Figure 8. ACES HP geometry.

2.6. Witness Plates

Witness plates were mounted behind all shots. The witness plates were of 0.5 mm thick Al 2024 T3 and were mounted 50 mm behind the target.

3. IMPACT TEST RESULTS SUMMARY

3.1. Fuel Pipes

16 normal (0° impact angle) HVI tests have been performed on FP. In ten tests, the pipe has been filled with water and pressurized with N_2 gas. In the other exps (experiments) the pipes were empty during impact. Tab. 1 lists the details of all FP exps: v_0 - impact velocity, d_P - projectile diameter, m_P - projectile mass, P_0 - pressure inside the pipe before impact, ΔP_{Max} - maximum measured overpressure. The damage class is given according to Dahl and Cour-Palais, 1991 (C2: no perforation, but with attached spall(s) or rear surface deformation; C3: no perforation, but with detached spall(s); C4: perforation, all hole diameters < 2 mm; C5: penetration, applicable if any hole diameter ≥ 2 mm).

Table 1. FP exps.

Exp	Conf.	v_0 [km/s]	d_P [mm]	m_P [mg]	P_0 [MPa]	ΔP_{Max} [MPa]	damage class
61	A25	5.8	1.25	2.9	—	—	C2
63	A25	6.1	1.25	2.9	—	—	C3
64	A25	6.2	1.25	2.9	2.9	(0.5)	C2
65	A25	5.9	1.25	2.9	2.9	(0.9)	C2
67	A25	5.7	1.5	5.4	3.0	—	C2
71	A25	6.2	2.0	12.0	3.1	0.8	C4
4595	A25	6.3	2.0	12.1	—	—	C4
93	M50	3.5	2.5	20.9	3.0	—	C2
72	M50	6.3	3.0	36.8	—	—	C2
4591	M50	6.2	3.5	58.3	—	—	C4
4588	M50	6.6	4.0	87.1	3.0	3.4	C2
4585	M50	6.8	5.0	176.1	3.0	> 10	C5
4592	M50	6.7	5.0	174.9	—	—	C4
4586	M100	2.7	3.5	58.8	3.0	1.6	C2
4587	M100	6.7	4.0	86.8	3.0	0.7	C4
4589	M100	7.8	3.5	58.8	3.0	2.9	C2

Exp 61 has been performed with a BP made of Al 6061 T4 instead of Al 6061 T6. Exps 4591, 4592 and 4595 have been performed with multiple pipes to increase probability of fragment impact. Two different pressure sensors were used to record pressure vs. time curves, a piezoceramic (Kistler 603B, used for ΔP_{Max}) and a piezoresistive (Kistler 4073A100, used for P_0). The overpressure of exp 4585 can only be estimated to ~ 15 to 25 MPa due to the pressure signal peak being cut off by the oscilloscope. In exps 64 and 65, only the 4073A100 was used, so the ΔP_{Max} values are not comparable and given in brackets for completeness only.

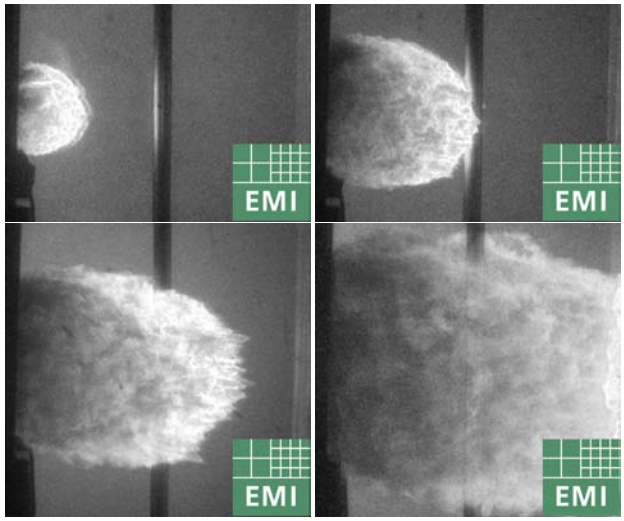

Figure 9. Optical Shadowgraphs / Digital High-Speed Photographs of exp 4585. Trigger times: 10, 15, 20, 30 µs wrt to impact on MLI.

3.2. Heat Pipes

14 normal (0° impact angle) HVI tests have been performed on HP. In eight tests, the pipes have been pressurized with N_2 gas. The two ACES HP were filled with high purity NH_3 and sealed by the manufacturer. They have been heated during the impact tests, inducing pressure. The pipes were empty during all other exps. Tab. 2 lists all HP exps: D_0 - projectile impact location to HP center offset. Damage is classified as either perforation or no perforation.

Table 2. HP exps. I = integrated, I-O = integrated with large projectile path offset, A = ACES.

Exp	Conf.	v_0 [km/s]	d_P [mm]	m_P [mg]	D_0 [mm]	P_0 [MPa]	ΔP_{Max} [MPa]	damage
92	A50	5.9	1.9	10.0	—	—	—	no p.
95	A50	5.9	2.5	20.9	—	—	—	no p.
4601	A50	6.7	3.0	36.3	—	4.5	< 0.1	perf.
4600	M50	6.3	3.5	58.9	—	4.5	< 0.1	perf.
4597	M50	6.2	5.0	176.8	—	—	—	perf.
4603	I	2.8	2.0	11.7	4	4.5	< 0.1	no p.
4607	I	3.0	2.0	12.0	1	—	—	perf.
4605	I	3.3	2.5	21.2	1	4.5	0.14	perf.
159	I	5.4	1.1	2.1	2	4.5	—	no p.
4602	I	6.7	1.5	5.2	1	4.5	< 0.1	perf.
4608	I-O	6.8	2.5	21.0	4	1.5	0.19	perf.
4609	I-O	6.8	2.5	20.9	14	4.5	< 0.1	no p.
4623	A	6.3	1.1	1.9	3	1.9	—	no p.
4640	A	6.9	3.5	58.5	3	2.0	—	perf.

Exp 4597 has been performed with three pipes. In exp 4603, the projectile did not penetrate the topmost heat pipe mounting profile, so the heat pipe itself is undamaged. Exp 4607 is very close to the BL (ballistic limit)

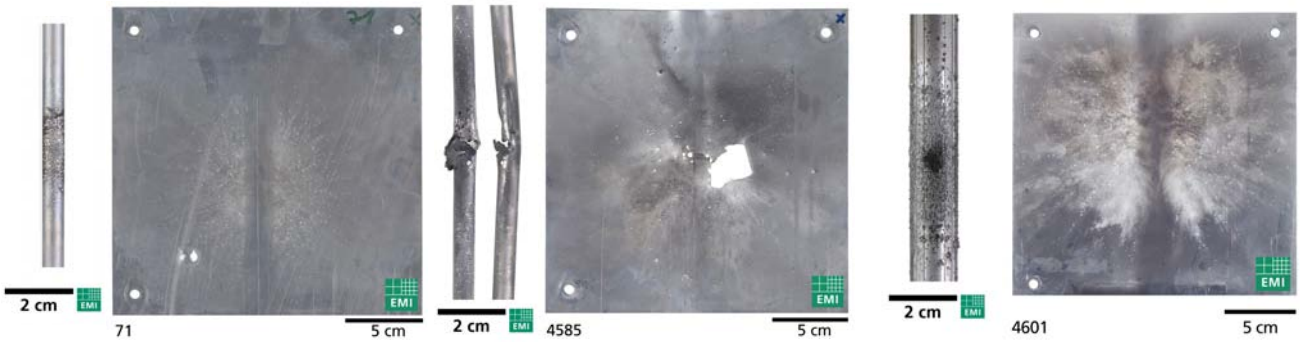

Figure 11. Fuel resp. heat pipe and witness plate damage of exps 71 (left), 4585 (center) and 4601 (right).

wrt (with regard to) perforation. The same pressure sensors as for the FP exps were used. For the ACES exps, P_0 is calculated from the heat pipe temperature.

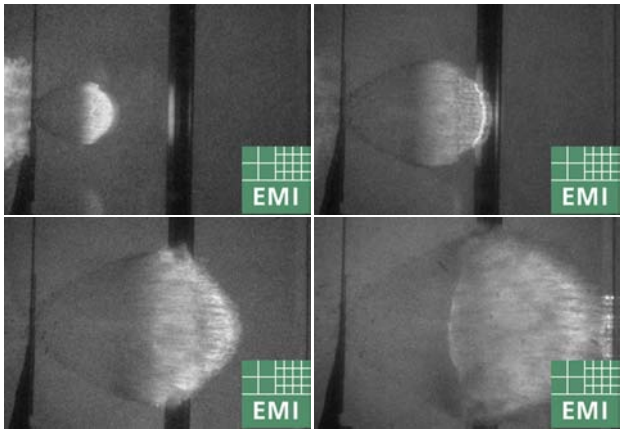

Figure 10. Optical Shadowgraphs of exp 4601. Trigger times: 5, 10, 15, 20 µs wrt to impact on BP.

4. BALLISTIC LIMIT

4.1. Fuel Pipes

Three different failure modes have been investigated on FP: detached spall, perforation and rupture. Detached spall and rupture were only observed once, so no BL is presented. However, the exps indicate that the pressurized liquid inside the pipes might have a slightly inhibitory effect on spallation.

The BL wrt perforation has been identified for all configurations at ~7 km/s. At impact velocities ~3 km/s, no pipe was impacted by a larger fragment, so no BL could be defined (see section 6 for an approach to deal this).

Fig. 12 shows the experimental results plotted against BL curves. The curves have been generated using the Christiansen Whipple Shield equation (Christiansen, 1993) and the EMI Triple Wall equation (Schäfer et al, 2005). It should be noted that these equations have been adjusted on set-ups of multiple plates; work on the equations is ongoing. The plotted curves show that both equations provide a conservative prediction.

The following data has been used for calculation of the BL curves: A25: t_B=0.81mm, ρ_B=2700kg/m^3, S=25mm; M50: S_{SP} =35mm, m_{SP}=3.45kg/m^2, S=50mm; M100: S_{SP}=35mm, m_{SP}= 3.45kg/m^2, S=100mm; all: ρ_P=2700kg/m^3, t_W=0.41mm, σ_Y= 724MPa. ρ_P - projectile density, t_B - BP thickness, ρ_B - BP density, S_{SP} - spacing between SP face sheets, m_{SP} - SP areal density, S - spacing between structure wall and pipe, t_W - pipe wall thickness, σ_Y - pipe wall tensile yield stress.

4.2. Heat Pipes

Two failure modes have been investigated: perforation and rupture. Detached spall was not considered a problem for HP because (1) any spall will stay inside the pipe and (2) contaminating the working fluid with small metallic fragments is not considered to affect a HP's operation. Rupture has not been observed as a failure mode; first signs of rupture show up in exp 4640.

The BL has been identified for the A50 configuration at ~7 km/s, for the integrated HP at 3 km/s and ~7 km/s, and roughly for the ACES HP at ~7 km/s. Fig. 13 shows the experimental results plotted against BL curves (calculated as for the fuels pipes). Due to the fairly complex geometry (see figs. 5, 7 and 8), two BL curves are given. The lower is calculated using the minimum wall thickness and provides a conservative prediction, while the upper is calculated with a larger wall thickness.

Exps 4608 and 4609 show that the integrated HP investigated improve the protective capabilities of the

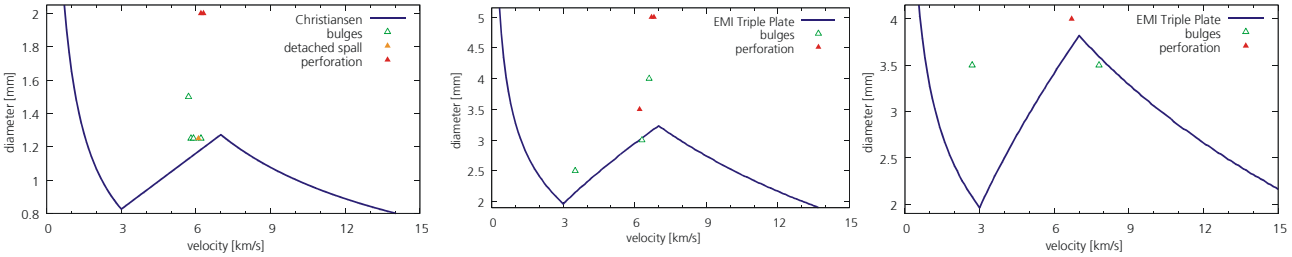

Figure 12. BL of fuel pipe configuration A25 (left), M50 (center) and M100 (right).

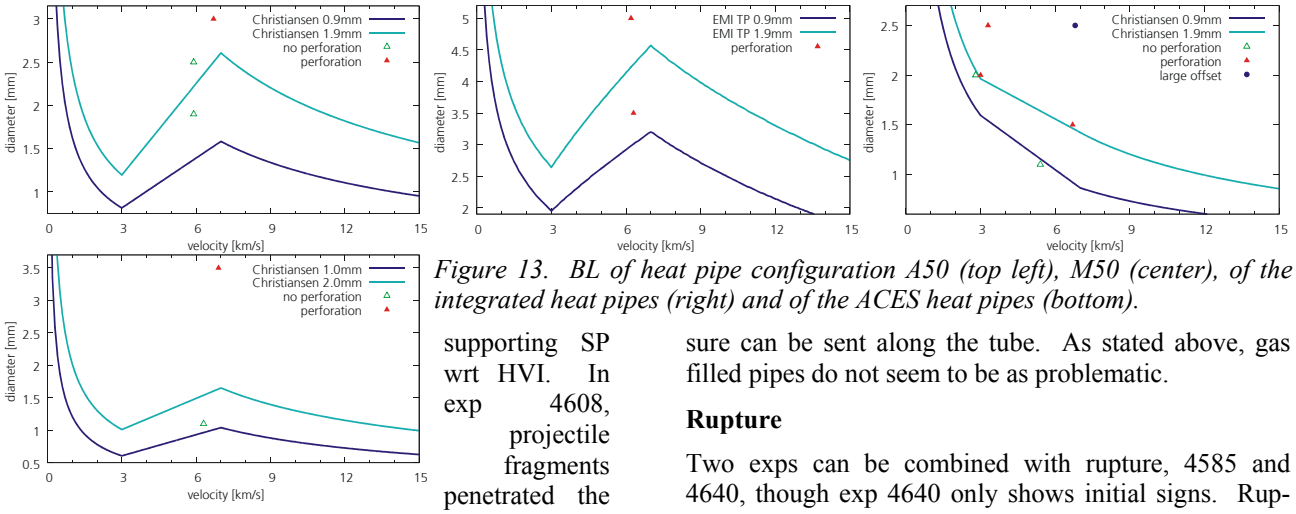

Figure 13. BL of heat pipe configuration A50 (top left), M50 (center), of the integrated heat pipes (right) and of the ACES heat pipes (bottom).

supporting SP wrt HVI. In exp 4608, projectile fragments penetrated the HP but were stopped in the pipe. In exp 4609, similar impact conditions with a larger miss distance lead to perforation of the SP, while the HP remained undamaged.

For the ACES HP, a similar conclusion can be made. The predicted BL of the SP alone at 7 km/s is ~0.8 mm, however, a 1.1 mm projectile was defeated by the pipe, thus the impact capability of the SP was improved.

The following data has been used for calculation of the BL curves: A50: t_B=0.80mm, ρ_B=2700kg/m^3, S=50mm; M50: S_{SP} =35mm, m_{SP}=3.45kg/m^2, S=50mm; integrated: t_B=2.3mm, ρ_B= 2770kg/m^3, S=8.2mm; all but ACES: ρ_P=2700kg/m^3, t_W=0.9 resp. 1.9mm, σ_Y=145MPa; ACES: ρ_P=2700kg/m^3, t_B=0.3mm, ρ_B=2710kg/m^3, S=10.4mm, t_W=1.0 resp. 2.0mm, σ_Y=160MPa.

5. OVERPRESSURE MEASUREMENTS

Comparison: Liquid Filled vs. Gas Filled Pipes

At similar impact conditions, liquid filled pipes experience a greater pressure peak than gas filled pipes. In exp 4585, d_P is approx. 1.5 times above the BL (for specific impact velocity), causing the liquid filled FP to rupture, and an overpressure roughly one order of magnitude above the operating pressure. In contrary, d_P in exp 4608 is approx. two times above BL (for specific impact velocity), however in this case the gas filled HP did not rupture, and the overpressure has approx. the same magnitude as the operating pressure.

Even fairly destructive exps with gas filled HP did not generate much overpressure inside the pipe, in comparison to destructive exps with fluid filled FP which produced considerable overpressure and rupture.

Threat to Adjacent Valves, Regulators etc.

Eps 4588 and 4585 show that overpressure inside liquid filled pipes may pose a threat for adjacent equipment. In exp 4588, the pipe was not perforated, but an overpressure peak of 3.4 MPa was measured. Exp 4585 shows that with severe impact conditions, a pressure pulse one order of magnitude above the operating pressure can be sent along the tube. As stated above, gas filled pipes do not seem to be as problematic.

Rupture

Two exps can be combined with rupture, 4585 and 4640, though exp 4640 only shows initial signs. Rupture is not really considered a problem, because (1) both exps are well above the BL for perforation, and (2) the energy released by the rupture of small pipes is negligible. Generally, rupture seems to occur mainly in combination with liquid rather than gas filled equipment.

6. FAILURE PROBABILITY

Exp 4586 shows a particularly large discrepancy between predicted and observed damage: d_P exceeds the predicted critical projectile diameter d_C by more than 50%, however the pipe did not fail as it was not impacted by a penetrating fragment. This discrepancy is likely to occur when the equipment is laterally confined and located behind a structure wall (e. g. BP or SP) and the fragment cloud consists of large fragments with a very inhomogeneous spatial distribution (i. e. at low velocities). So far, no approach to deal with this situation has been published.

6.1. Definitions

The failure probability of laterally bounded equipment following an impact ($P_{f,Equip}$) is equal to the product of three probabilities: (1) the probability of MOD impacts on the S/C structure wall in the vulnerable area of the considered equipment ($P_{I,Struct}$), (2) the probability that the downrange fragment cloud hits the equipment ($P_{I,Equip}$), and (3) the probability of failure of laterally unbounded equipment behind the structure walls ($P_{f,\infty}$):

$$P_{f,Equip} = P_{I,Struct} \cdot P_{I,Equip} \cdot P_{f,\infty} \quad (1)$$

$P_{I,Struct}$ is found via risk analysis tools (e. g. ESABASE). $P_{f,\infty}$ can be calculated using existing BL equations:

$$P_{f,\infty} = \begin{cases} 1, & d_P \geq d_C \\ 0, & d_P < d_C \end{cases} \quad (2)$$

To calculate $P_{I,Equip}$, different assumptions are made, depending on the projectile velocity v_0.

Assumptions for Failure Probability, $v_0 \geq 7$ km/s

In the hypervelocity regime ($v_0 \geq 7$ km/s) it is assumed that (1) the fragment cloud spreads over an angle of 2 β,

(2) the equipment fails if it is hit by the fragment cloud (and $d_P \geq d_C$), and (3) the equipment remains intact if it is located outside the fragment ejection cone (or $d_P < d_C$).

β allows definition of a "vulnerable area" on the structure wall. The lateral extension $2 \cdot R$ of this area is defined by the spacing S between target and structure wall, β, the target diameter d_T, and d_P:

$$2 \cdot R = 2 \cdot (S \cdot \tan \beta + \tfrac{1}{2} (d_T + d_P)) \qquad (3)$$

see Fig. 14. This vulnerable area can (when d_P is small) be marked upon the S/C structure wall (Fig. 14 right).

To actually calculate R, an assumption on β is needed. For this, the fragment cloud leading edge velocity is estimated to be equivalent to v_0, and the fragment cloud radial velocity is estimated to be ½ v_0. This leads to β = arctan ½ ≈ 27°. Exps 4591, 4592, 4595 and 4597 show that the major damage is inside an angle of ~ 10° to 25°, depending also on d_P / d_C.

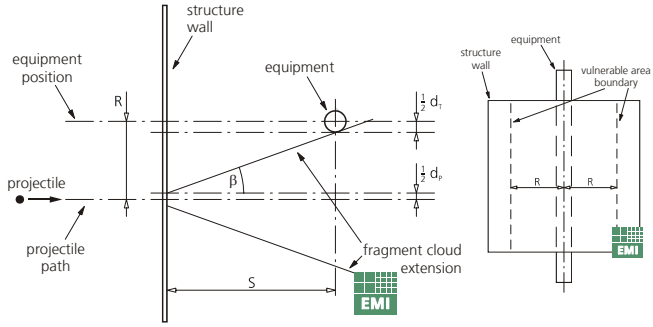

Figure 14. Left: Definition of the "vulnerable area". Right: Boundary of the "vulnerable area", view perpendicular onto the structure wall.

Assumptions for Failure Probability, $v_0 \leq 3$ km/s

In the ballistic regime ($v_0 \leq 3$ km/s), the following assumptions are made: (1) the projectile is not fragmented, (2) the equipment fails, if hit by the projectile (and $d_P \geq d_C$), and (3) the equipment remains intact, if not hit by the projectile (or $d_P < d_C$). Thus, the impact probability wrt the vulnerable area calculates to

$$P_{I,Equip} = \frac{d_P + d_T}{2 \cdot R} \qquad (4)$$

6.2. Failure Probability Function

Between the hypervelocity and ballistic regimes, $P_{I,Equip}$ is interpolated linearly with v_0. This results in the following overall probability function:

$$P_{I,Equip} = \begin{cases} (d_P + d_T) / 2\,R, & v_0 \leq 3 \text{ km/s} \\ \text{interpolation} & \text{in between} \\ 1, & v_0 \geq 7 \text{ km/s} \end{cases} \qquad (5)$$

Fig. 15 shows an example plot of $P_{I,Equip}$ for a pipe located behind a BP: d_T=6.35mm, S=25mm, ρ_P=2700 kg/m^3, t_B=0.81mm, ρ_B=2700kg/m^3, t_W=0.41mm, σ_Y= 724MPa.

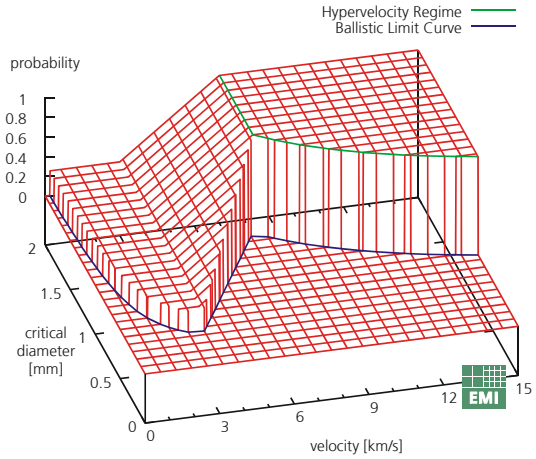

Figure 15. Example probability function.

7. CONCLUSIONS

The vulnerability of space qualified fuel pipes and heat pipes has been assessed. The equipment was placed behind representative spacecraft structure walls. During a part of the experiments, it has been operated under representative conditions.

Ballistic limit curves for the failure mode perforation have been derived for all investigated configurations. Other failure modes have been investigated but are not considered to be important.

Large overpressures were recorded in the experiments with liquid filled fuel pipes. The gas filled heat pipes do not seem as susceptible to overpressures.

An approach to deal with the failure probability of laterally confined equipment behind structure walls was presented.

ACKNOWLEDGEMENT

All of the work presented in this paper has been done under ESA contract 16483/02. Work on the contract is still in progress.

REFERENCES

Christiansen, Eric L.: Design and performance equations for advanced meteoroid and debris shields, *Int. J. Impact Engng*, Vol. 14, 145-156, 1993.

Dahl, Kim V.; Cour-Palais, Burt G.: Standardization of impact damage classification and measurements for metallic targets, to be published, 1991.

Janovsky, R.; Kalninsch, I.; Stichternath, A.: The Meteoroid and Debris Protection System for the ATV-Spacecraft, 50th International Astronautical Congress, Amsterdam, The Netherlands, October 1999.

Schäfer, F.; Putzar, R.: Triple Wall Ballistic Limit Equation, this volume, 2005.